Effect of filler metal and post-weld friction stir processing on stress corrosion cracking susceptibility of Al–Zn–Mg arc welds

T. E. Borchers[1], A. Seid[2], S. S. Babu[3], P. Shafer[2] and W. Zhang*[1]

Localised T (tau) phase precipitation at the weld toe of gas metal arc welds was correlated to stress corrosion cracking in the lap joints of aluminium alloy (AA) 7003 (Al–Zn–Mg) welded with AA 5356 (Al–Mg) type filler wire. To further investigate the detrimental effect of T phase precipitates on cracking initiation, two strategies were developed. First, welds were made with AA 4043 (Al–Si), eliminating the T phase precipitation, while maintaining similar heat affected zone characteristics. Second, the toe region of Al–Zn–Mg weld, made with AA 5356 filler wire, was post-weld friction stir processed through which the T precipitates were displaced and encapsulated in a subsurface region, isolating those precipitates from the surface corrosive environment. For both cases, an increase in cracking resistance was demonstrated. The impact of processing on joint strength was discussed based on the lap shear tensile testing data.

Keywords: Aluminium alloys, Gas metal arc welding, Stress corrosion cracking, Friction stir processing, 7xxx series, Al–Zn–Mg, Finite element analysis

This paper is part of a special issue on Problems in the Welding of Automotive Alloys

Introduction

Decreasing the weight of vehicles is of particular interest to the automotive industry for increased fuel economy. Priority on low cost, high volume production leads to the demand for arc weldable, strong, lightweight alloys such as 7xxx series aluminium alloys (AAs). High strength Al–Zn–Mg–Cu 7xxx series AAs are typically considered 'unweldable' by fusion welding processes due to their strong susceptibility to solidification or 'hot' cracking. Although it has been shown that scandium (Sc) addition to filler wire[1] or base metal[2] can significantly mitigate hot cracking due to grain refinement, welding application of those Cu bearing high strength AAs in automotive structures has been limited. On the other hand, medium strength Cu–lean, Al–Zn–Mg 7xxx series AAs are 'weldable' lightweight alloys that have been evaluated for automotive structural applications.[3] 5xxx series (Al–Mg) filler wires are typically used when welding these Cu–lean 7xxx series alloys to avoid hot cracking.[4,5]

The largest drawback from using these alloys is the fact that when exposed to a combination of corrosive environment and tensile stress state, Al–Zn–Mg welded structures become prone to stress corrosion cracking (SCC). Previous studies[6–8] have shown that SCC propagates in the heat affected zone (HAZ) or along the fusion line of the 7xxx series weldment. Also notable, relevant SCC failures initiate in the weld toe.[9,10] The complex mechanism for SCC in AAs is still debated,[11,12] but evidence suggests that anodic dissolution of secondary phase precipitates [e.g. η ($MgZn_2$) intermetallic phase] and hydrogen embrittlement are both factors contributing to SCC.[11–17] It is generally agreed that the following three conditions must be present for SCC to occur: (i) susceptible microstructure is exposed to (ii) aggressive environment under (iii) tensile stress above some threshold value.

In authors' previous work,[6] AA 7003-T4 lap joints welded with AA 5356 filler wire were investigated for cracking when exposed to a corrosive environment and under a bending load. It was observed that the cracking consistently initiated at the weld toe, which was enriched with Mg.[18] Such segregation of Mg resulted in formation of continuous precipitation of T (tau) phase, $Mg_{32}(Al,Zn)_{49}$, on grain boundaries in the weld toe, and absent elsewhere in the bulk weld metal. The cracking mechanism was identified as SCC since the crack did not occur if any of the necessary conditions (i.e. stress, environment and microstructure) were removed. For instance, the sample did not fail without loading in the corrosive environment. When testing in air under bending, the sample failed in a different manner. Finally, when the microstructure was altered by completely removing T phase by means of milling away the entire weld toe, the sample did not crack in stress corrosion testing. It was thus hypothesised that preferential dissolution of the continuous T precipitation in the weld toe is fundamentally responsible for SCC *initiation* in some welded Al–Zn–Mg alloys since this phase is more electrochemically active than the Al matrix phase.[13,19] It is noted that the mechanism for

[1]The Ohio State University, Columbus, OH, USA
[2]Honda R&D Americas Inc., Raymond, OH, USA
[3]Department of Mechanical, Aerospace and Biomedical Engineering, University of Tennessee, Knoxville, TN, USA

*Corresponding author, email zhang.3978@osu.edu

© 2015 Institute of Materials, Minerals and Mining
Published by Maney on behalf of the Institute
Received 5 December 2014; accepted 16 December 2014
DOI 10.1179/1362171814Y.0000000273

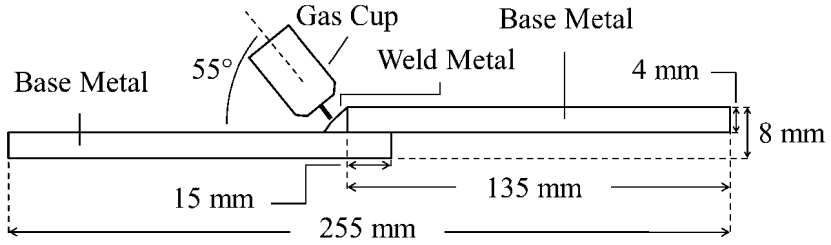

1 Schematic of robotic welding sample set-up

SCC *propagation* was not investigated, as the complexity of SCC in the dissimilar metal weldment may lead to differing mechanisms for crack initiation and propagation.

The purpose of the present study is to test the proposed hypothesis,[6] improving the understanding of SCC initiation in welded 7xxx series AAs. Two methods are used to alter the T phase in the weld toe. The first method uses a 4xxx series (Al–Si) filler wire, as opposed to 5xxx series (Al–Mg), during arc welding to alter the chemical composition of the weld toe while maintaining a similar HAZ and joint geometry.

Instead of forming T phase, the 4xxx series weld toe microstructure will likely contain Si rich phases such as α-Al_8Fe_2Si, β-Al_5FeSi, π-$Al_8FeMg_3Si_6$, (Si) and/or Mg_2Si.[20] These precipitates are also common to 6xxx series (Al–Mg–Si) alloys. Owing to low relative thermodynamic stability in the presence of Si, phases containing Zn are not expected to precipitate, and any Zn from the base material will remain in solid solution. Electrochemical analysis shows that precipitates containing Fe and Si tend to be cathodic or neutral to the aluminium matrix.[21] For example, using a 0·1 n calomel reference electrode, the potentials of Mg_2Si and Si are −0·83 and −0·26 V respectively. For comparison, the potential of a 99·95% pure Al matrix is −0·85 V. Hence, these phases would not be expected to undergo anodic dissolution, which in turn, can help suppress SCC initiation in the weld toe.

The second method to alter T phase precipitates is post-weld friction stir processing (FSP) of the 5xxx series weld toe such that the weld toe is placed in the centre of the stir zone (nugget). It is noted that a large number of studies have been reported on the SCC susceptibility of friction stir welded/processed AAs. For instance, a study on AA 5454 showed SCC resistance in friction stir welded joints, while gas tungsten arc welds were susceptible to SCC.[22] On the other hand, both the weld nugget and HAZ outside of the processed region in AA 7050 showed susceptibility to SCC in the form of intergranular corrosion.[23] The published study on FSP of arc welds is limited. The thermal–mechanical conditions in FSP are expected to result in the following changes to the arc weld. First, the grain size will be reduced in the FSP nugget region, a phenomenon commonly observed in FSP due to dynamic recrystallisation.[24] Second, depending on the Mg and Zn compositions at the weld toe, the T precipitates may dissolve into solution[25] or coarsen if stable to the melting temperature. Finally, threaded tools impart a downward flow known as a Maelstrom current[26] leading to material near the centre of the tool (weld toe) depositing deeper into the joint.

In the present study, samples are prepared by the aforementioned two methods (i.e. 4xxx series filler wire and post-weld FSP) and are then tested for SCC susceptibility in a cyclic corrosion chamber. The testing results are compared with the existing data for samples welded with AA 5356 filler wire. The critical role of T precipitates on SCC initiation at the weld toe is then discussed. Finally, the impact of using 4xxx filler wire and post-weld FSP on the joint strength is discussed based on the results from lap shear tensile testing.

Experimental

Details of welding procedure are available,[6] and a brief summary is provided in the following. Samples used for testing were lap joints with 15 mm overlap created by joining two extruded AA 7003-T4 measuring $135 \times 125 \times 4$ mm in dimension. The gas metal arc welding (GMAW) process was conducted with a 55° angle to the horizontal and a 10° push angle. A schematic of this set-up is pictured in Fig. 1. The filler wires used were AA 5356 (Al–Mg) and AA 4043 (Al–Si); both wires had a diameter of 1·2 mm. Nominal compositions of the base material and filler wires are displayed in Table 1. The shielding gas was commercially pure argon. For welds made with AA 5356, the average welding wirefeed speed was set to 12·5 m min^{-1} with ± 1 m min^{-1} pulses at 10 Hz; the welding travel speed was 0·75 m min^{-1}. For AA 4043, the average welding wirefeed speed was set to 7·6 m min^{-1} with ± 1 m min^{-1} pulses at 10 Hz; the welding travel speed was also 0·75 m min^{-1}. The lower wirefeed speed was used to account for the higher electrical conductivity of AA 4043. Welding was performed using a Motoman robot interfaced with a Fronius power supply.

The stress corrosion testing was performed based on a cyclic corrosion testing (CCT) method in accordance with a custom, more rigorous variation of ASTM B117-11, Standard Practice for Operating Salt Spray (Fog) Apparatus. The welded sample was loaded in a rigid bending fixture under a constant displacement (Fig. 2).

Table 1 Nominal composition range of base material AA 7003, filler wire AA 5356 and filler wire AA 4043

	Al	Mg	Zn	Si	Cr	Cu	Fe	Mn	Ag	Ti	Zr
AA 7003	Bal.	0·5–1·0	5·0–6·5	0·3	0·2	0·2	0·35	0·3	0·25–0·4	0·2	0·25
AA 5356	Bal.	4·5–5·5	0·1	0·25	0·05–0·2	0·1	0·4	0·05–0·2	0	0·06–0·2	0
AA 4043	Bal.	0·2	0·1	4·5–6·0	0	0·3	0·6	0·15	0	0·15	0

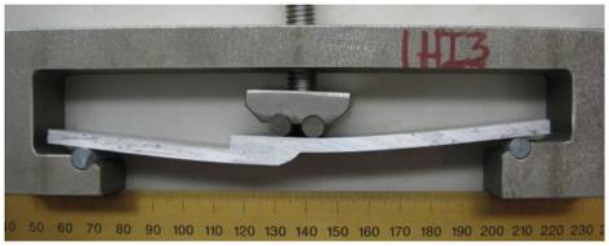

2 Example of sample under 5 mm displacement in rigid fixture for SCC testing

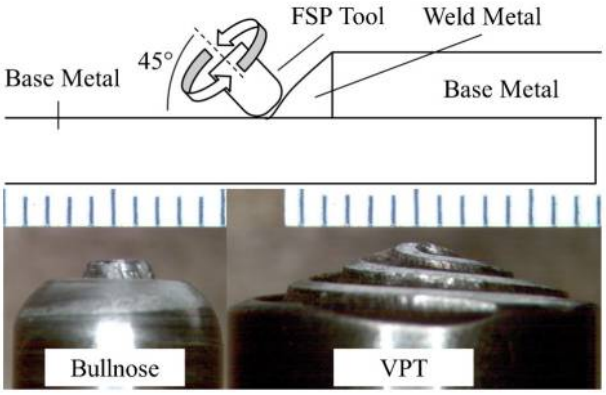

3 Schematic FSP of weld toe with side views of VPT and bullnose tool designs (scale in millimetres)

The fixture was electrically isolated from the sample. To ensure the applied stress at the weld toe region was above the threshold stress for SCC, a displacement as high as 5 mm was used, resulting in plastic deformation of the sample. In other words, the applied stress at the weld toe was expected to be at or beyond the room temperature yield strength of the base metal. The prestressed samples were placed inside a CCT chamber, which cycled through periods of salt spray (fog) exposure and non-exposure and periods of low (−20°C) and high temperatures (60°C). The corrosive medium used was a 5%NaCl aqueous solution. The samples were taken out periodically to examine the existence of surface cracks. Samples that did not crack in the CCT chamber after 40 to 50 days were considered as non-cracking and were removed from the chamber for further post-test metallography examination.

Post-weld FSP of the weld toe was conducted using two different tool designs. As shown in Fig. 3, one design was a variable penetration tool (VPT) that had a cone shaped pin with coarse thread. The other design was a 'bullnose' tool, which had a tapered cylindrical pin with a rounded circumferential edge and fine thread. The radius of the VPT design was 7·94 mm, and that of the bullnose design was 4·76 mm. A schematic of the set-up for FSP of a welded sample is also shown in Fig. 3. The tool was plunged into the weld toe at an angle of 45° to the horizontal and traversed across the entire length of the weld. The rotational velocity for both the VPT and bullnose designs was set to 3000 rev min^{-1}. Displacement control was used with a depth of vertical penetration set to 0·64 mm.

Joint strength of the as welded samples and the post-weld FSP samples was determined by tensile testing with a lap shear configuration following the JIS standards Z2241 and Z3136.

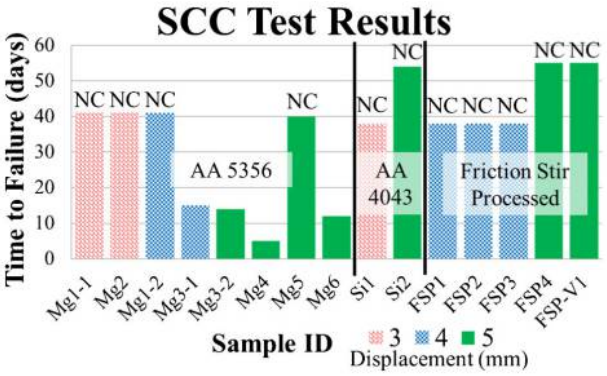

4 Comparison of SCC susceptibility of various samples (*x* axis) at different strain levels (displacements) in as welded AA 5356, AA 4043 or FSP geometries, where 'NC' stands for 'no crack'

For metallographic examination, samples were cold mounted in epoxy, polished and then etched with Keller's reagent. The optical microscope used for characterisation was the Olympus GX51. Energy dispersive X-ray spectroscopy (EDS) was performed on the FEI Quanta 200 scanning electron microscope.

Results and discussion

Lap joint samples in three different conditions (as welded AA 5356, as welded AA 4043 and post-weld FSP AA 5356) were tested in the CCT chamber. For brevity of referencing to sample conditions, the following nomenclature is used (Fig. 4). Sample names started with Mg, e.g. Mg1–2 or Mg2, correspond to the as welded samples welded with AA 5356 (Al–Mg) filler wire. Similarly, the samples welded with AA 4043 (Al–Si) filler metal are denoted as Si1 and Si2. For the trailing numbers in the name, the first digit signifies the weld plate number. If multiple samples were machined from the same plate, their names are designated by the second digit. For instance, Mg3–1 and Mg3–2 are two samples that were cut from the same weld plate, no. 3. The samples welded with AA 5356 followed by a post-weld FSP using the 'bullnose' tool are denoted as FSP1, FSP2, FSP3 and FSP4; each was machined from a different post-weld FSP plate. Finally, the sample welded with AA 5356 followed by a post-weld FSP using the variable penetrant tool is denoted as FSP-V1. Figure 4 summarises the SCC testing results in terms of the time to failure for various samples and loading conditions. Samples that did not crack within 40 to 50 days of exposure in CCT chamber were removed from the environment and labelled, NC, to indicate no cracking.

Although, the above results have confirmed our hypothesis that changing the filler wire to 4xxx series and FSP have mitigated the SCC, the following sections discuss the sensitivity of SCC resistance with reference to local microstructures and stress concentrations. Finally, the impact of using AA 4043 filler wire and post-weld FSP with reference to joint strength is also discussed.

Correlation of local microstructure to SCC susceptibility

As welded AA 5356

As shown in Fig. 4, the as welded AA 5356 samples (denoted as Mg1–1 etc.) show a high susceptibility to

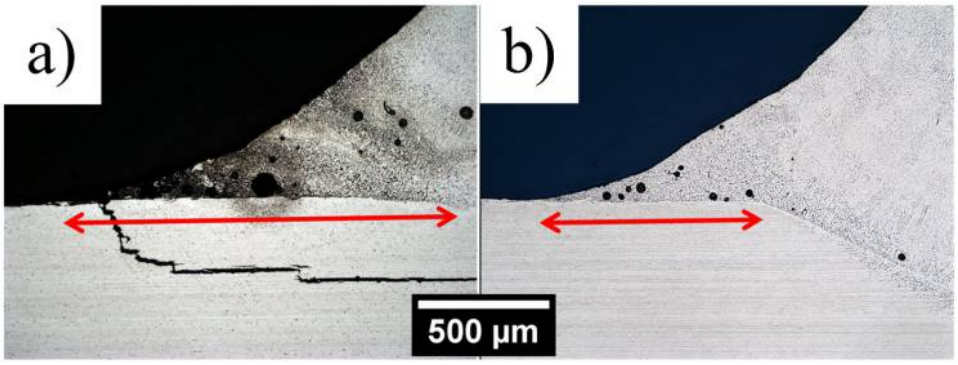

a Mg3–2; *b* Mg1–2

5 Comparison of optical micrographs of weld toe region in cracked and uncracked samples

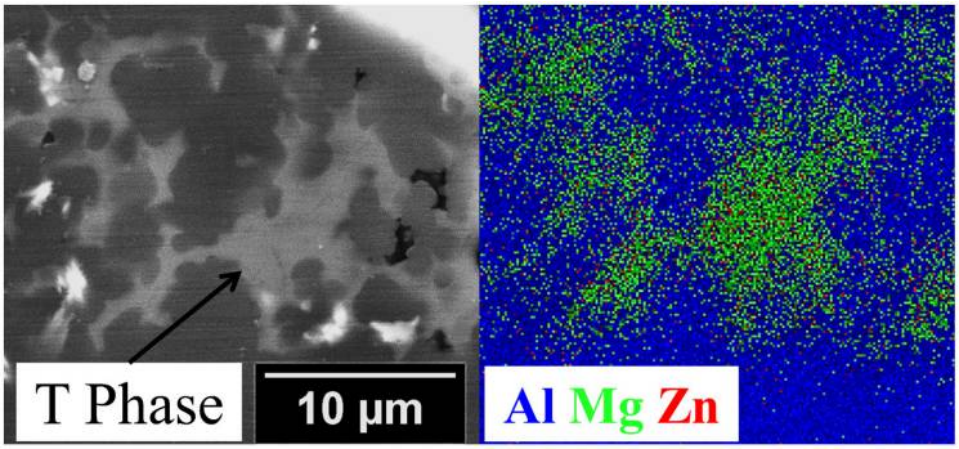

6 Backscattered electron image of continuous T phase along grain boundaries and corresponding EDS map of same region

SCC when they were displaced to either 4 or 5 mm in the rigid bending fixture (Fig. 2). Those samples failed within 15 days of exposure in the CCT chamber. On the other hand, none of the AA 5356 samples displaced to 3 mm cracked in the CCT chamber; this is attributed to the lower stress/strain state (below the threshold value for SCC) across the weld toe.

Some variability in testing results is observed in the AA 5356 samples. In particular, Mg1–2 and Mg5 were displaced to 4 and 5 mm respectively, yet neither cracked within 40 days of exposure in the CCT chamber. Such variability is likely caused by the variation in microstructure at the weld toe region, as discussed in the following. Figure 5 shows the optical micrographs for the cracked sample Mg3–2 and the uncracked sample Mg1–2. The weld toe region is examined since it corresponds to the region where the stress corrosion crack initiated. As reported in authors' previous work,[18] precipitates of $Mg_{32}(Al,Zn)_{49}$ T phase, which is anodic to the Al matrix, existed along the grain boundaries at the weld toe of the cracked AA 5356 samples. For completeness, a backscattered electron image of such continuous T precipitates at the weld toe and the corresponding composition map are shown in Fig. 6. In the present study, both cracked and uncracked samples after SCC testing were carefully cleaned and then etched using Keller's reagent for the same duration of time. The cracked sample, for which T phase precipitates existed at the weld toe, corroded severely due to etching, whereas the uncracked sample corroded slightly. Such marked difference in the corrosion response due to etching indicates a different microstructure existed at the weld toe of the uncracked sample.

It is noted that the grain boundary T precipitates were found to be confined to the overlapping region at the weld toe in the previous work.[18] The overlapping region, marked by the arrow in Fig. 5, corresponds to the weld toe where the fusion line is flat (i.e. no weld penetration). Such overlapping region seems to result from the weld metal wetting the base metal surface. As shown in Fig. 5, the width of the overlapping region for the uncracked sample is ~50% that of the cracked sample. The shorter overlapping region is consistently observed in other uncracked samples.

In summary, the variability in SCC susceptibility for AA 5356 is likely caused by the 'local' microstructure variation at the weld toe, possibly a lower fraction of T precipitates in the smaller overlapping region for uncracked samples. Such difference in microstructure is attributed to the inherent variability of the GMAW process between welding trials despite using the same welding parameters.

As welded AA 4043

Samples welded with AA 4043 (Al–Si) filler wire exhibit resistance to SCC (Fig. 4). In particular, samples Si1 loaded to 3 mm displacement and Si2 loaded to 5 mm displacement were removed from the CCT chamber

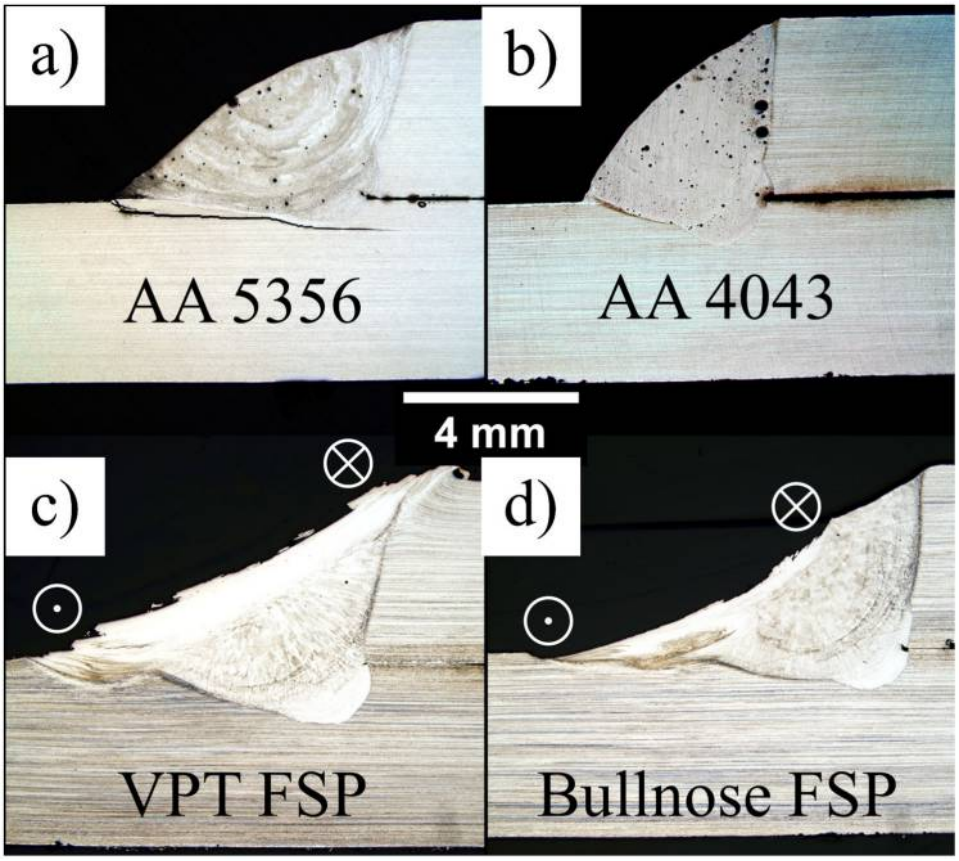

a Mg3–1; *b* Si2; *c* FSP-V1; *d* FSP4

7 Macrographs of SCC tested lap joint samples where advancing and retreating sides of FSP are indicated by 'x' and dotted circles respectively

after exposure for 38 and 54 days without cracking respectively. A macrograph of sample Si2 is shown in Fig. 7*b*, and a zoomed in view of the weld toe region is further shown in Fig. 8*b*. A comparison of weld bead geometry shows that the AA 4043 weld in Fig. 7*b* has a larger weld toe angle (142°) than the AA 5356 weld (125°) in Fig. 7*a*. The stress concentration factor for Si2 is thus expected to be higher than that for Mg3–1. Hence, the improved resistance to SCC in AA 4043 samples is primarily due to the weld toe microstructure since the corrosion environment and the tensile stress condition in AA 4043 samples are the same as (if not worse than) those in AA 5356 samples. In particular, there is an obvious discrepancy between how the etchant corroded samples Si2 and Mg3–1. The sample welded with AA 4043 does not exhibit preferential corrosion at the weld toe.

To understand the possible microstructure that existed in the AA 4043 weld metal, non-equilibrium solidification calculations based on the Scheil equation were performed using two commercial computational thermodynamics software packages: ThermoCalc with SSOL4 database and JMatPro with AA database. The composition of liquid metal was approximated by a dilution calculation involving the AA 4043 filler wire and AA 7003 base metal resulting in 20% base metal with 80% filler wire. The notable intermetallic phases predicted to precipitate on solidification are (Si), α-Al_5FeSi), π-$Al_8FeMg_3Si_6$ and Mg_2Si; the weight fractions predicted for these precipitates were 3·5, 2·0, 0·3 and 0·3% respectively. These phases are either neutral or cathodic to the aluminium matrix,[21] so anodic dissolution of these grain boundary precipitates cannot occur. Hence, the 'inert' precipitates in the weld toe of AA 4043 samples are expected to be much more resistant to SCC when compared to the 'active' T precipitates in AA 5356 samples.

Friction stir processing of AA 5356 samples

Owing to the difficulty in maintaining desirable surface finish using the variable penetrant tool at an inclined angle, only one 'good' sample was machined from the FSP plate for testing in the CCT chamber. As shown in Fig. 7*c*, the processed surface is relatively discontinuous with numerous sharp corners even for this good sample (FSP-V1). Such sharp corners (or notches) can potentially promote crack initiation due to the high stress concentration. Despite the unfavourable surface geometry, sample FSP-V1, loaded to a large displacement of 5 mm, was removed from the CCT chamber after exposure for 55 days without cracking. Figure 8*c* shows a zoomed in view of the weld toe region in which a severe surface defect is observed at the location where the stir zone meets the base metal. The existence of this and other surface defects did not lead to the initiation and propagation of SCC in the FSP sample.

Samples processed with the 'bullnose' tool had better surface finish when compared to those processed using the VPT. A typical macrograph of the processed joint and the zoomed in view of the weld toe region are shown in Figs. 7*d* and 8*d* respectively. The 'bullnose' processed sample surface is relatively continuous although there is a shallow undercut (~200 μm deep) at the weld toe. As

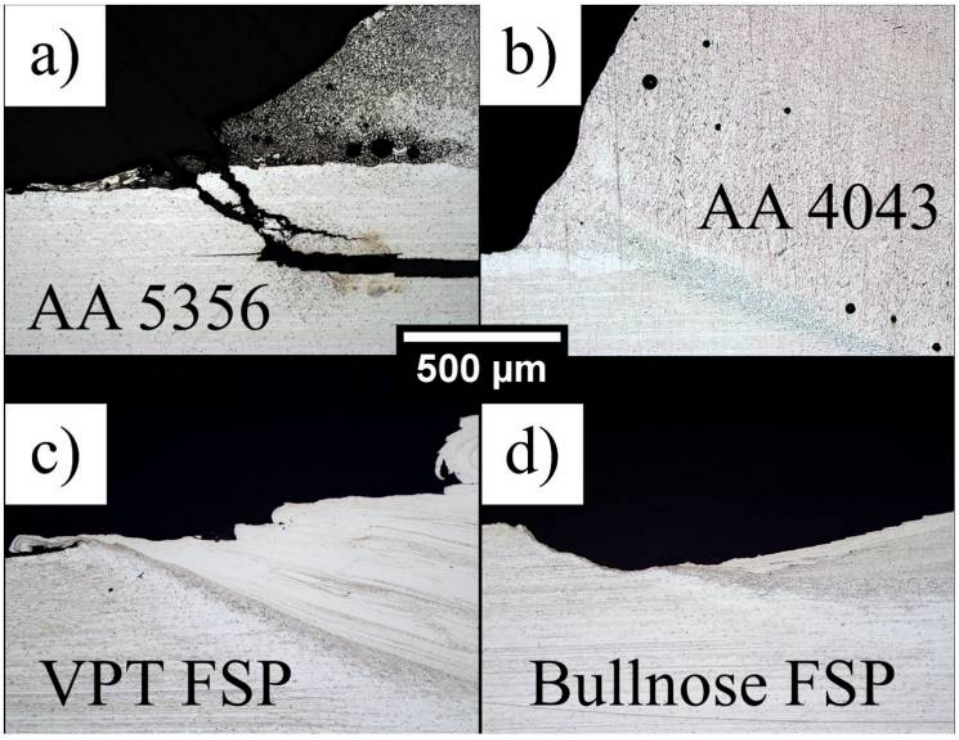

a Mg3–1; *b* Si2; *c* FSP-V1; *d* FSP4

8 Micrograph cross-sections at weld toe of SCC tested lap joints samples

9 Stitched micrographs of sample FSP1 where lack of fusion, 'weld toe remnant' and location of EDS linescan vector are indicated

shown in Fig. 4, the 'bullnose' processed samples are strongly resistant to SCC. Samples FSP1, FSP2 and FSP3, all loaded to a 4 mm displacement, were removed from the corrosive environment after 38 days of exposure without signs of cracking. Sample FSP4, loaded to a 5 mm displacement, was further tested for 55 days of exposure and was not found to exhibit cracking.

A large area view of sample FSP1 is shown in Fig. 9, where several interesting observations can be made. First, the processed surface is relatively discontinuous due to the aforementioned difficulty in FSP at an inclined angle. A sharp crack is observed on the left side of the image. This crack is determined to be a lack of fusion defect (occurred during the FSP) rather than SCC due to the following reason. The typical stress corrosion crack in as welded AA 5356 samples is intergranular and surrounded by regions corroded severely when exposed to etchant (Fig. 8*a*). The crack in sample FSP1 did not exhibit an intergranular morphology, and the surrounding region did not corrode significantly when etched.

Another interesting observation in Fig. 9 is a dark region ~700 μm below the sample surface. This region is located right beneath root hole/defect due to FSP and appears to be dark due to preferential etching. To assess the composition in the dark region, an EDS linescan was performed along the vector denoted 'linescan vector' in Fig. 9. The compositional results indicate a strong increase in Mg from 2 wt-% outside the dark region up to 15 wt-% in the dark region. Given the qualitative nature of EDS, the composition for the dark region at the bottom of the stir zone is consistent to that of T precipitate rich weld toe in as welded AA 5356 samples reported previously.[18] In other words, this dark region is likely composed of the 'weld toe remnant' that was displaced downwards by ~700 μm during FSP. Such resulting weld toe remnant is observed in each of the FSP samples, including sample FSP-V1 processed by the VPT.

In summary, the following microstructural changes are observed in the post-FSP arc weld with AA 5356 filler wire. The grain size in the nugget was significantly decreased as expected. The T phase did not dissolve, nor did it coarsen. Rather, it was stirred/displaced deeper into the weld due to the Maelstrom material flow driven by the threaded pin.[26] The T precipitates seem to maintain the general shape and constitution after FSP possibly due to the short time exposure to high temperature.

Correlation of SCC to local stress state

It is noted that FSP, especially using the bullnose tool, resulted in a smoother weld toe profile (Fig. 7) and thus

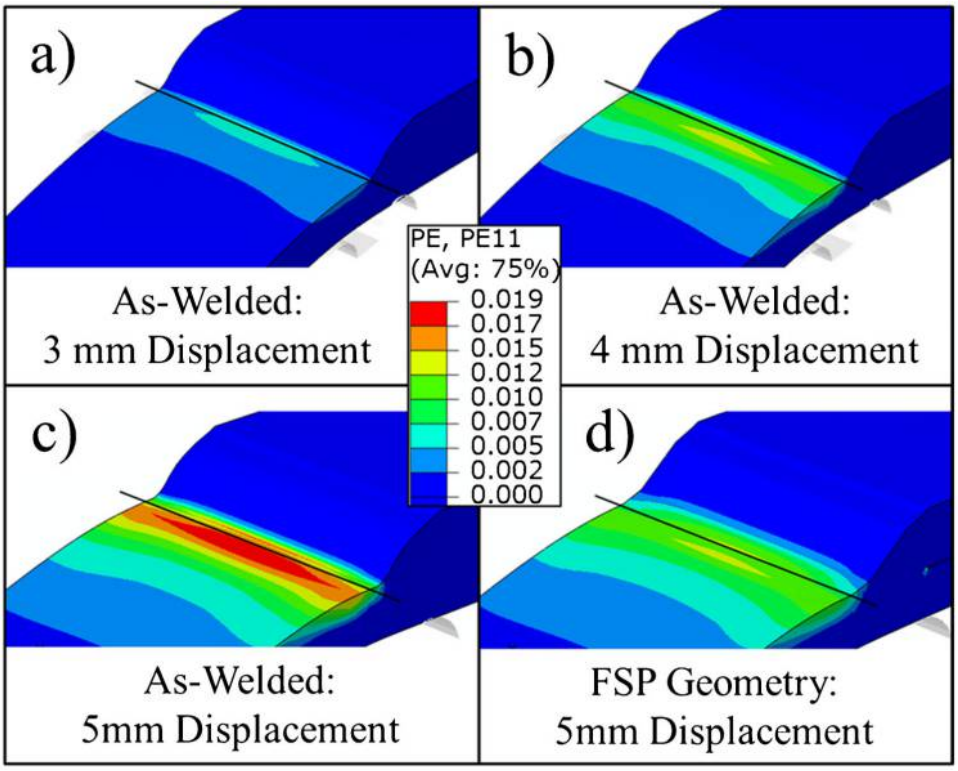

a 3 mm; *b* 4 mm; *c* 5 mm; *d* FSP geometry (5 mm)

10 Abaqus FEA models comparing tensile plastic strain between various displacements of as welded geometry where thin black line represents location of fusion line in each model

a lower stress concentration factor at the weld toe. In order to assess the effect of geometry on the stress/strain state, a finite element analysis (FEA) was conducted using the commercial software Abaqus. Model geometries were obtained by digitising the optical macrographs of as welded and FSP samples shown in Fig. 7*a* and *d* respectively. The digitised coordinates were then used to create a 3D mesh of the two samples.

The fixture used for CCT testing was represented by rigid bodies in the model. Simple mechanical interactions were defined between the rigid bodies and the sample. Displacement was applied to the rigid body as it would in the actual fixture, and the resulting stress and strain fields in the sample were calculated.

Two main simplifications were used in the present model. First, the residual stress from welding and/or FSP was not considered. Second, simple elastic–plastic property data for the base metal and the filler metal were assigned to the base plate and the weld bead respectively. The modelling results were calibrated with strain data measured on physical samples loaded in the fixture. As a result, the calculated plastic strain was used as a first approximation of the threshold value for SCC.

Figure 10*a* and *b* shows the calculated plastic strain fields for the as welded geometry displaced to 3 and 4 mm respectively. This is the strain component that is transverse to the welding direction. These results are used to determine the threshold value of plastic strain to induce SCC, as discussed in the following. The SCC test results (Fig. 4) show that samples displaced to 3 mm did not develop cracks, whereas samples displaced to 4 mm exhibited failure in SCC testing. In other words, the threshold value of stress/strain for SCC lies in between those displaced to 3 and 4 mm. The FEA results show the magnitude of plastic strain at the fusion line (marked by the black line) is $7{\cdot}74 \times 10^{-3}$ after 3 mm of displacement and $12{\cdot}60 \times 10^{-3}$ after 4 mm. It is thus concluded that joint geometries exhibiting at least $12{\cdot}60 \times 10^{-3}$ plastic strain at the fusion line are above the threshold value for SCC; geometries exhibiting $<7{\cdot}74 \times 10^{-3}$ plastic strain are below the threshold for SCC.

Figure 10*c* and *d* shows the as welded and FSP samples displaced to 5 mm respectively. Both geometries experience substantial plastic deformation across the fusion line. In particular, the magnitude of calculated plastic strain at the fusion line in the as welded geometry is $19{\cdot}38 \times 10^{-3}$, and in the FSP geometry is $13{\cdot}13 \times 10^{-3}$. Although the magnitude in the FSP model is lower than that in the as weld geometry, it is still above the threshold determined previously. Hence, the reduction in stress concentration due to smoother toe profile after FSP is not expected to have a significant effect on decreasing SCC. The improved resistance to SCC after post-weld FSP is thus likely caused by the displacement of anodic T precipitates to the interior and resulting isolation from the surface environment.

Correlation of process modifications to joint strength

The stress-strain curves tested in the lap shear tensile testing condition are plotted in Fig. 11. The as welded AA 5356 had an ultimate tensile strength ~260 MPa, which is comparable to the nominal value of the filler metal. The post-weld FSP decreased the joint strength by 10–15%; this reduction in strength is attributed to the decrease in throat size of the weld joint. The as welded AA 4043 had the lowest ultimate tensile strength (130 MPa). Such low joint strength is expected because

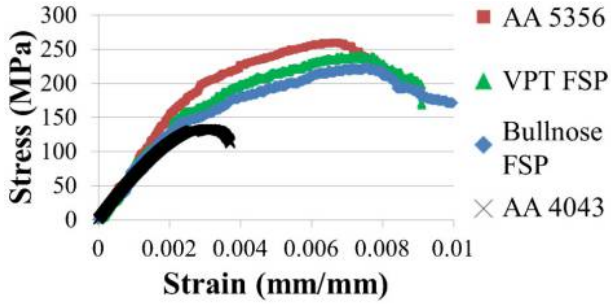

11 Lap shear tensile testing results of as welded (AA 5356 and AA 4043) and FSP geometries

the AA 4043 filler wire itself is relatively soft with a nominal ultimate tensile strength of 145 MPa. For all geometries, failure initiated at the weld root and propagated through the weld throat. This is expected due to the lower strength of the filler wires compared to AA 7003 base metal.

Conclusions

Stress corrosion cracking in AA 7003 lap joint welded with AA 5356 filler wire was correlated to continuous T phase precipitates along the grain boundaries at the weld toe, as reported in the previous study.[18] In the present study, variability in SCC testing results of AA 5356 samples was analysed by comparing the local microstructure at the weld toe. In particular, samples with SCC failure had weld toes that etched preferentially when exposed to the Keller's reagent. The preferential etching correlated with the location of T phase precipitates. On the other hand, a noticeable preferential etching was not observed in the uncracked samples that were displaced to 4 and 5 mm in CCT. Hence, the variability in SCC is attributed to difference in local microstructure, which is further caused by the inherent variability of the GMAW process.

To further study the effect of T precipitates on SCC, two methods were used to alter the microstructure. The Al–Si filler wire, AA 4043, was used to alter the chemical composition in the weld toe, eliminating the possibility for T phase to precipitate. The second method, post-weld FSP of the weld toe, successfully displaced and isolated the T precipitates, previously in the weld toe, from the surface, effectively isolating the T precipitates from the corrosive environment. The resulting microstructures from both methods were found to be resistant to SCC. The results from a FEA indicate that SCC resistance of the FSP samples is not due to the improved weld toe profile since the tensile plastic strain is still above the threshold value.

Despite increased SCC resistance, welding with AA 4043 should not be utilised where a substantial joint strength is necessary. The FSP of the AA 5356 weld joint also increased the SCC resistance and minimally reduced the strength. However, difficulty in implementation of post-weld FSP into mass production manufacturing can limit this method as a practical engineering solution. Nevertheless, the results of this investigation have led to an improved understanding of the SCC phenomenon in 7xxx series AA welds, especially in recognising the detrimental effect of continuous T phase precipitation along grain boundaries on the initiation of SCC of Al–Zn–Mg weldments.

Acknowledgements

This research work was supported financially by Honda R&D Americas Inc. through the Center for Integrative Materials Joining Science for Energy Applications (CIMJSEA), a National Science Foundation's Industry & University Cooperative Research Center. Mr Z. Pramann and Mr W. Al-Fakir are acknowledged for conducting the post-weld FSP at EWI facilities. The CCT was conducted at the Honda R&D Americas Inc. facilities. Andrea Peer of Ohio State University aided in the microstructural investigation.

References

1. A. F. Norman, S. S. Birley and P. B. Prangnell: *Sci. Technol. Weld. Joining*, 2003, **8**, 235–245.
2. G. M. Reddy, A. K. Mukhopadhyay and A. S. Rao: *Sci. Technol. Weld. Joining*, 2005, **10**, 432–441.
3. J. Dabrowski, M. Bruhis and J. R. Kish: 'Effect of corrosoin on the strength of fillet arc welded Cu-lean AA7xxx joints', in 'Supplemental proceedings: volume 2: materials properties, characterization, and modeling', 437–444; 2012, Hoboken, NJ, USA, John Wiley & Sons, Inc.
4. S. Yang and Q. Lin: *Adv. Mater. Res.*, 2011, **148–149**, 640–643.
5. M. G. Mousavi, C. E. Cross, O. Grong and M. Hval: *Sci. Technol. Weld. Joining*, 1997, **2**, 275–278.
6. T. E. Borchers, A. Seid, W. Zhang, P. Shafer, S. S. Babu and D. H. Phillips: 'Stress corrosion cracking susceptibility of gas metal arc welded 7xxx series aluminum alloys', Proc. Sheet Metal Welding Conf. XVI, American Welding Society, Detroit, MI, USA, 2014, 3B–5.
7. S. Kou: 'Welding metallurgy', 2nd edn; 2003, New York, Wiley.
8. C. M. Liao: *Corrosion*, 1993, **49**, 52–59.
9. M. C. Reboul, B. Dubost and M. Lashermes: *Corros. Sci.*, 1983, **25**, 999–1018.
10. A. K. Jha, G. N. Shiresha and K. Sreekumar: *Eng. Fail. Anal.*, 2008, **15**, 787–795.
11. T. D. Burleigh: *Corrosion*, 1991, **47**, 89–97.
12. R. Braun and T. Hack: 'Werkstoffwoche '96, Symposium 7: Materialwissenshaftliche Grundlagen', (eds. F. Aldinger and H. Mughrabi); 1997, Frankfurt, Germany, DGM-Informationsgesellshaft Verlag.
13. M. Baumgartner and H. Kaesche: *Corrosion*, 1988, **44**, 231–239.
14. M. O. Speidel: *Met. Trans. A*, 1975, **6A**, 1975.
15. S. P. Lynch: *Acta Metall.*, 1988, **36**, 2639.
16. D. Najjar, T. Magnin and T. J. Warner: *Mater. Sci. Eng. A*, 1997, **A238**, 293–302.
17. N. J. H. Holroyd and G. M. Scamans: *Metall. Mater. Trans. A*, 2013, **44A**, 1230–1253.
18. T. E. Borchers, D. P. McAllister and W. Zhang: 'Macroscopic segregation and stress corrosion cracking in 7xxx series aluminum alloy arc welds', *Metallurgical and Materials Transactions A*. 2015, **46**, 1827–1833.
19. M. C. Carroll, M. J. Mills and R. G. Buchhiet: '5000 series alloys with improved corrosion properties and methods for their manufacture and use', US 2004/0091386 A1, May 13, 2004.
20. N Coniglio, C. E. Cross, I. Dorfel and W. Osterle: *Mater. Sci. Eng. A*, 2009, **A517**, 321–327.
21. M. Textor, J. Timm and P. Nema: *Materialwiss. Werkstofftech.*, 1995, **26**, 318–326.
22. G. S. Frankel and Z. Xia: *Corrosion*, 1999, **55**, 139–150.
23. J. B. Lumsden, M. W. Mahoney, C. G. Rhodes and G. A. Pollock: *Corrosion*, 2003, **59**, 212–219.
24. A. Tronci, R. McKenzie, R. M. Leal and D. M. Rodrigues: *Sci. Technol. Weld. Joining*, 2011, **16**, 433–439.
25. J. Yan and A. P. Reynolds: *Sci. Technol. Weld. Joining*, 2009, **14**, 582–587.
26. A. C. Nunes, Jr.: 'Wiping metal transfer in friction stir welding', Aluminum 2001: Proc. 2001 TMS Annual Meeting Automotive Alloys and Joining Symp., New Orleans, LA, USA, 2001, Minerals, Metals, and Materials Society (TMS), Warrendale, PA, USA, 235–248.